3.11 TURBULENT TRANSFER COEFFICIENTS AND ROUGHNESS LENGTHS OVER SEA ICE: THE SHEBA RESULTS

Edgar L Andreas[1*], Christopher W. Fairall[2], Andrey A. Grachev[3], Peter S. Guest[4], Thomas W. Horst[5], Rachel E. Jordan[1], and P. Ola G. Persson[3]

[1]U.S. Army Cold Regions Research and Engineering Laboratory, Hanover, New Hampshire
[2]NOAA Environmental Technology Laboratory, Boulder, Colorado
[3]Cooperative Institute for Research in Environmental Sciences, University of Colorado, Boulder, Colorado
[4]Naval Postgraduate School, Monterey, California
[5]National Center for Atmospheric Research, Boulder, Colorado

1. INTRODUCTION

On the night of 30 January 1998, the ice cracked around the Canadian icebreaker *Des Groselliers* and severed the power lines than ran the SHEBA ice camp. Lights went out in the camp, and data collecting stopped at our main 20-meter Atmospheric Surface Flux Group (ASFG) tower for almost eight days. Despite this breakup and many others, the experiment to study the Surface Heat Budget of the Arctic Ocean (SHEBA) still produced the largest and most comprehensive set of surface-level meteorological and turbulence data ever collected over sea ice.

Andreas et al. (1999) and Persson et al. (2002) describe the instruments that our group deployed and maintained in and around the SHEBA camp. For example, besides that main tower, we always had three or four remote portable automated mesonet (PAM) stations deployed in the vicinity of the camp. These were Flux-PAM stations designed and built by NCAR's Integrated Surface Flux Facility. Since these were self-contained, during the breakup, they continued recording despite the power outage in the main camp. Here we report analyses of the eddy-correlation measurements of the momentum and sensible heat fluxes that we made through the SHEBA year at our main tower and at these PAM stations.

The momentum flux or surface stress (τ) and the sensible heat flux (H_s) couple the lowest levels of the atmosphere to the sea ice surface and, thus, serve as some of the boundary conditions for mesoscale and large-scale atmospheric models. Such models typically estimate these turbulent surface fluxes with a bulk flux algorithm formulated as

$$\tau = \rho C_{Dr} U_r^2 , \qquad (1a)$$

$$H_s = \rho c_p C_{Hr} U_r \left(\Theta_s - \Theta_r\right) . \qquad (1b)$$

Here, ρ is the air density; c_p, the specific heat of air at constant pressure; U_r, the wind speed at reference height r; Θ_s, the potential temperature at the surface; and Θ_r, the potential temperature at height r.

The set (1) usually includes a third equation—one for the latent heat flux. But since the Flux-PAM stations did not measure the latent heat flux directly and since our eddy-correlation measurements of that flux on our main tower have, so far, proved inscrutable, we do not discuss parameterizations for the latent heat flux here. Instead, see Andreas (2002) or Andreas et al. (2003).

The secret to the bulk flux algorithm is evaluating the turbulent transfer coefficients in (1): C_{Dr} is the drag coefficient appropriate at reference height r, and C_{Hr} is the transfer coefficient at height r for sensible heat. For example, NCAR's Climate System Model (Bryan et al. 1996) uses a formulation like (1) over both open ocean and sea ice surfaces. C_{Dr} and C_{Hr} change with the surface, however. Here we use our SHEBA measurements to learn better how to estimate C_{Dr} and C_{Hr} over sea ice surfaces. We call our resulting synthesis the SHEBA bulk flux algorithm.

Corresponding author address: Edgar L Andreas, U.S. Army Cold Regions Research and Engineering Laboratory, 72 Lyme Road, Hanover, NH 03755; e-mail: eandreas@crrel.usace.army.mil.

2. FORMAL BACKGROUND

As a consequence of Monin-Obukhov similarity theory, we can formally write C_{Dr} and C_{Hr} in (1) as

$$C_{Dr} = \frac{k^2}{\left[\ln\left(\frac{r}{z_0}\right) - \psi_m\left(\frac{r}{L}\right)\right]^2} , \qquad (2a)$$

$$C_{Hr} = \frac{k^2}{\left[\ln\left(\frac{r}{z_0}\right) - \psi_m\left(\frac{r}{L}\right)\right]\left[\ln\left(\frac{r}{z_T}\right) - \psi_h\left(\frac{r}{L}\right)\right]} . \qquad (2b)$$

Here, k is the von Kármán constant, which we take as 0.40 for our analysis, but see Andreas et al. (2002). Also in (2), ψ_m and ψ_h are "known" corrections for near-surface atmospheric stratification effects that depend on the stability parameter $\zeta \equiv r/L$, where L is the Obukhov length. For unstable stratification ($\zeta < 0$), we use Paulson's (1970) functions for ψ_m and ψ_h; for stable stratification ($\zeta > 0$), we use Holtslag and De Bruin's (1988) functions.

At our main tower and at the PAM stations, we measured all the quantities in (1) except C_{Dr} and C_{Hr}. We can therefore evaluate these from the measurements. But, at least according to (2), the roughness lengths for wind speed (z_0) and temperature (z_T) seem to be more fundamental variables. And, in fact, developing theoretical expressions for z_0 and z_T is often easier than treating C_{Dr} and C_{Hr} theoretically.

Consequently, having evaluated C_{Dr} and C_{Hr} from the data, we can invert (2) to obtain values for z_0 and z_T. That is,

$$z_0 = r \exp\left\{-\left[k C_{Dr}^{-1/2} + \psi_m(\zeta)\right]\right\} , \qquad (3a)$$

$$z_T = r \exp\left\{-\left[k C_{Dr}^{1/2} C_{Hr}^{-1} + \psi_h(\zeta)\right]\right\} . \qquad (3b)$$

Realize that we also know L, and thus ζ, from our measurements; therefore, computing z_0 and z_T from our data is straightforward.

Once we know z_0 and z_T, we can compute the transfer coefficients in more standard form. To make comparing data from various sites and for various surfaces meaningful, we usually report C_D and C_H at a standard reference height of 10 m. Likewise, for such comparisons, we prefer to remove stratification effects to compare surface properties more fairly. From (2), we see that for neutral stability (when $\psi_m = \psi_h = 0$) and for a 10-m reference height,

$$C_{DN10} = \frac{k^2}{\left[\ln(10/z_0)\right]^2} , \qquad (4a)$$

$$C_{HN10} = \frac{k^2}{\left[\ln(10/z_0)\right]\left[\ln(10/z_T)\right]} . \qquad (4b)$$

These are the so-called neutral-stability transfer coefficients appropriate for a reference height of 10 m. Clearly, knowing z_0 and z_T is equivalent to knowing the neutral-stability transfer coefficients.

3. THE ROUGHNESS LENGTH z_0

3.1 Overview of the Year

Our instruments ran at SHEBA from October 1997 through September 1998. All the data that we report here are based on hourly averages for this period.

Figure 1 shows a time series for the SHEBA year of C_{DN10} values measured at our main tower and at the Flux-PAM stations called Atlanta, Baltimore, and Florida. The PAM stations made eddy-correlation measurements of τ and H_s at one level only. Our main tower measured at five levels; all the tower values that we report here, however, are based on the median values of the available flux measurements from the five levels.

Because of riming problems with the sonic anemometer/thermometers on the PAM stations that were not corrected until March or April 1998, the data returns from these early in the experiment were spotty. Figure 1 therefore shows monthly averages of C_{DN10} values from the PAM stations until March 1998 (SHEBA day 425 is 1 March 1998). In Fig. 1, for all the tower data and for the PAM stations starting in March, the plotted points are averages for the first 10 days of the month, for the second 10 days, and for the remainder of the month.

We identify two aerodynamic regimes in Fig. 1. From the start of the experiment through 14 May 1998 (day 499), the sea ice was snow covered, and the snow was dry enough to drift.

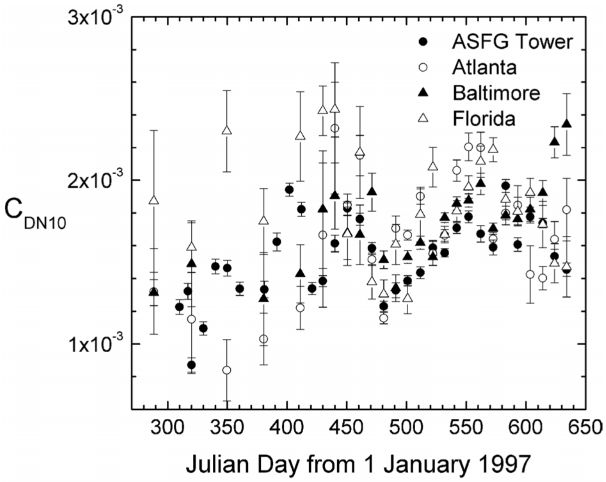

Figure 1. Neutral-stability, 10-m values of the drag coefficient from four SHEBA sites. Depending on the data available, we averaged hourly C_{DN10} values either monthly or by thirds of a month. Error bars are two standard deviations of the mean.

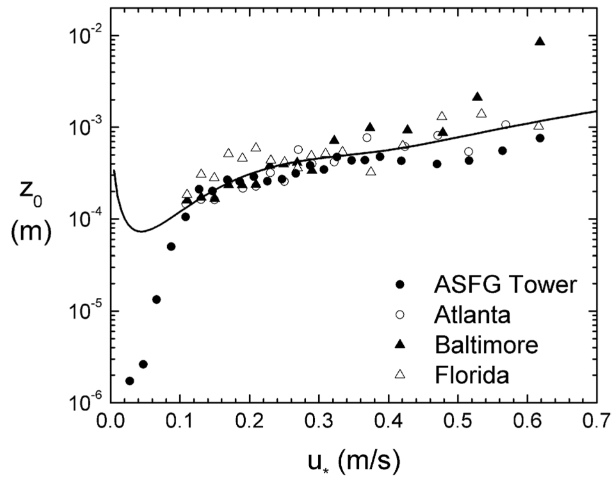

Figure 2. Bin-averaged z_0 values for winter from the main Atmospheric Surface Flux Group tower and from three Flux-PAM sites. The curve is (5).

We call these conditions winter. These conditions resumed and winter thus returned (aerodynamically speaking) on 15 September 1998 (day 623). The C_{DN10} values during this period are quite scattered, which we suspect is a wind effect. (The scanty data from the PAMs early in this period could also explain the scatter, though.)

When the snow got sticky, stopped drifting, and eventually melted, however, the four sites depicted in Fig. 1 agree much better as to the value of C_{DN10}. Surprisingly, when the snow was gone from the ice and the surface became pockmarked with melt ponds and leads, the sea ice appeared more aerodynamically homogeneous than a snow-covered surface. Hence, we treat the non-drifting and snow-free period, 15 May through 14 September 1998 (days 500–622), as an aerodynamic regime we call summer. Henceforth, we partition our data and analyses into winter and summer.

3.2 z_0 in Winter

Figure 2 shows bin-averaged z_0 values for winter (October 1997 through 14 May 1998 and 15 September to October 1998) measured on our main tower and at the three PAM stations with the most continuous records. The bins are 2 cm s^{-1} wide in u_* for the smaller u_* values and 5 cm s^{-1} wide for the larger values, where we had fewer observations.

This figure summarizes over 6,200 hourly z_0 values measured at the four sites. Most markers represent the average of many hourly z_0 values—sometimes over 200. Only a couple of markers in the highest u_* bins are based on one or two values.

The curve in the figure is

$$z_0 = \frac{0.135\,\nu}{u_*} + 2.0\times10^{-4}\exp\left[-\left(\frac{u_* - 0.25}{0.15}\right)^2\right] + \frac{0.03\,u_*^2}{g} \quad ,(5)$$

where ν is the kinematic viscosity of air and g is the acceleration of gravity. Equation (5) gives z_0 in meters when the other variables are in MKS units.

Equation (5) is similar to expressions that Jordan et al. (2001) and Andreas et al. (2003) use to model z_0 for snow-covered sea ice on Ice Station Weddell. It suggests three aerodynamic regimes: an aerodynamically smooth regime where z_0 goes as ν/u_*, a drifting snow regime where energy arguments (Owen 1964) suggest z_0 scales with u_*^2/g, and an intermediate regime between these extremes where the "permanent" roughness of the surface dictates the momentum transfer. In essence, (5) is similar to the two-term summation that Smith (1988) and Fairall et al. (1996) use to model z_0 over the open ocean. Our result, however, has a third term, the middle term on the right, that accounts for the fundamental roughness of the surface.

We chose the coefficients in the second and third terms in (5) specifically to fit the z_0 data in Fig. 2. These tuning values are similar to but not exactly the same as in the expressions that Jordan et al. (2001) and Andreas et al. (2003) report. We are still studying the reasons for these differences.

The data in Fig. 2 do not seem well represented at low u_* by the aerodynamically smooth relation, the first term on the right of (5). But measuring both u_* and z_0 in very light winds is difficult because, in the Arctic, such conditions are usually variable, and the turbulence is often intermittent. We thus rely on wind tunnel measurements for this end of our parameterization.

3.3 C_{DN10} in Summer

Figure 3 has three panels. The top panel repeats the C_{DN10} values from Fig. 1 from the late winter through the end of the experiment. This series highlights the fairly consistent behavior of the C_{DN10} values among the four sites during the summer.

As summer progressed at SHEBA, leads opened in the vicinity of the camp, all the snow melted, and the sea ice surface became increasingly pocked with melt ponds. The water features, in particular, created edges that the wind could push against. That is, form drag, which is sustained by pressure forces on the near-vertical ice faces (e.g., Banke et al. 1980; Andreas et al. 1984; Andreas 1995; Birnbaum and Lüpkes 2002), becomes a significant mechanism for air-surface momentum transfer in the summer. Our observations that the C_{DN10} data in Fig. 1 converge better in summer than in winter suggest that form drag may dominate the momentum exchange in summer.

Since open water is associated with the vertical edges that created this form drag, in the middle panel of Fig. 3, we show the lead fraction of total surface area in the vicinity of the SHEBA camp, the melt pond fraction, and the total open water fraction (the sum of leads and ponds). These data are courtesy of D. K. Perovich (2001, personal communication). The C_{DN10} data seem to follow the trend in the total water fraction. C_{DN10} is low in mid-May 1998 when the ice is still snow covered. But C_{DN10} begins increasing as open water appears in late May (day 517 is 1 June 1998) and peaks near the maximum in open water fraction. C_{DN10} then returns to typical winter values as the open water freezes and becomes snow covered.

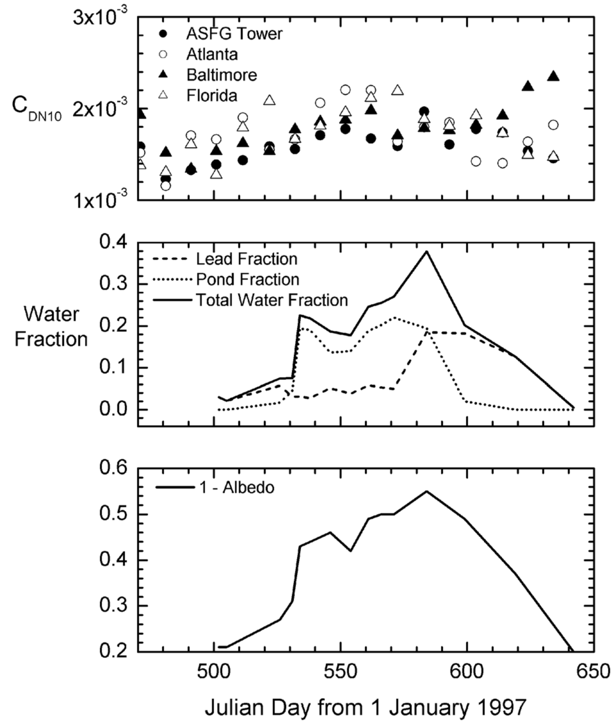

Figure 3. The top panel shows C_{DN10} values from Fig. 1, though without error bars, for the SHEBA summer of 1998. The middle panels shows total open water fraction in the vicinity of the SHEBA ice camp and the contributions to this from leads and melt ponds. The bottom panel is one minus the areally averaged albedo that D. K. Perovich (2001, personal communication) inferred from the observed surface types.

The peak in summer C_{DN10} does not coincide perfectly with the peak in total water fraction. It is quite close, however, to the peak in pond fraction; but C_{DN10} does not fall off beyond the peak as rapidly as the pond fraction does. Perhaps C_{DN10} reflects a weighted sum of lead and pond coverages rather than just the total water fraction.

The bottom panel in Fig. 3 suggests that the areally averaged albedo may also be a predictor for C_{DN10}. These albedo values also come from D. K. Perovich (2001, personal communication) and derive from his measurements of surface types and their individual albedo values. The lower two panels in Fig. 3 suggest that we may be able to estimate C_{DN10} from satellite observations.

We therefore pursue the relationship between summer C_{DN10} and ice concentration (or equivalently, water fraction) in Fig. 4. Here we have interpolated the C_{DN10} values in Fig. 3 to the corresponding water fraction, W, and, subsequently, to

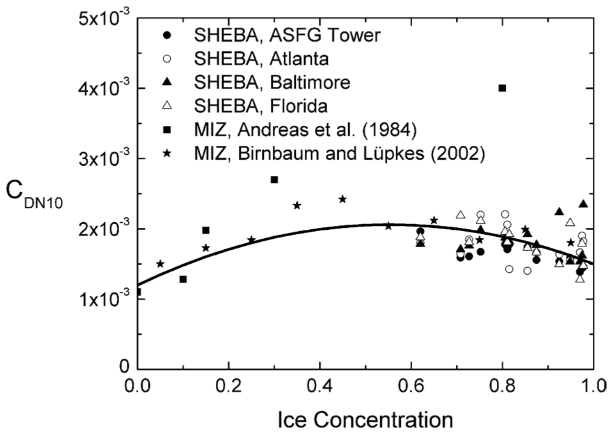

Figure 4. C_{DN10} values as a function of ice concentration. The four SHEBA sites are for summer observations only. The data from Andreas et al. (1984) and Birnbaum and Lüpkes (2002) are from measurements in the marginal ice zones in the Antarctic and the Arctic, respectively. The curve is (6).

the ice concentration, $C=1-W$. Remember, C is the areal coverage of bare ice. There is, of course, ice at the bottom of the melt ponds that is not included in this value.

The data in Fig. 4 tend to support our contention that C_{DN10} increases as the ice concentration decreases from 100% and more edges emerge. But for SHEBA, the ice concentration was always greater than 60% (Figs. 3 and 4). Therefore, to complete the picture of how C_{DN10} depends on ice concentration, we add two more data sets to complement the SHEBA data in Fig. 4. These are observations in the Antarctic marginal ice zone near the Greenwich Meridian that Andreas et al. (1984) made and a more extensive aircraft survey in the Arctic marginal ice zone near Svalbard that Birnbaum and Lüpkes (2002) report. These two sets are not necessarily summer observations; but since we are primarily interested in edge effects related to open water, they do not have to be.

We fitted the observations in Fig. 4 with a second-order polynomial,

$$10^3 C_{DN10} = 1.20 + 3.11C - 2.81C^2 , \qquad (6)$$

where C is the fractional ice concentration. Equation (6) suggests that C_{DN10} peaks at 2.06×10^{-3} when $C=0.55$. Realize, though, that this fit depends somewhat on our choice of endpoints—namely, the values of C_{DN10} over the open ocean ($C=0$) and over compact sea ice ($C=1$), which we took as 1.20×10^{-3} and 1.50×10^{-3}, respectively. In essence, Fig. 4 shows a unified picture of how C_{DN10} depends on ice concentration, whether the ice surface is the marginal ice zone or the central pack in summer.

4. THE ROUGHNESS LENGTH z_T

4.1 Background

The roughness length for temperature, z_T, in (2b) is analogous to z_0: it is the fictitious height at which the temperature profile meets the surface temperature Θ_s. From (4), we see that knowing z_0 and z_T is equivalent to knowing C_{DN10} and C_{HN10}. But devising theoretical models for z_T is easier than modeling C_{HN10} directly (e.g., Brutsaert 1975; Liu et al. 1979; Andreas 1987). Hence, we focus our discussion on the behavior of z_T or z_T/z_0 since z_T/z_0 appears in

$$C_{HN10} = \frac{C_{DN10}}{1 - k^{-1} C_{DN10}^{1/2} \ln\left(z_T / z_0\right)} , \qquad (7)$$

which derives from (4).

Equation (7) shows that, when $z_T = z_0$, the neutral-stability transfer coefficients for momentum and sensible heat are the same. This equality is essentially the Reynolds analogy (e.g., Schlichting 1968, p. 268 f.). The stability-dependent transfer coefficients in (2) need not be the same, though, because the stratification corrections, ψ_m and ψ_h, may be different.

Andreas (1987) developed a model for z_T/z_0 that is still the only theoretical prediction for how z_T behaves over surfaces of snow and ice. That model predicts z_T from

$$\ln\left(z_T / z_0\right) = b_0 + b_1\left(\ln R_*\right) + b_2\left(\ln R_*\right)^2 , \qquad (8)$$

where $R_* = u_* z_0 / \nu$ is the roughness Reynolds number. Andreas (1987) and Andreas (2002) tabulate the polynomial coefficients in (8) for flow that is aerodynamically smooth, in transition, or aerodynamically rough.

Andreas (2002) reviews some limited tests of the validity of (8) for both z_T and z_Q, the roughness length for humidity. Andreas et al. (2003) report on how results from a more extensive data set, collected over snow-covered Antarctic sea ice, compare with (8) for both z_T and z_Q. Here we describe how the SHEBA z_T data compare with (8).

4.2 z_T in Winter

Figure 5 shows z_T values measured on our main tower during the winter and plotted as (8) suggests. The data are quite scattered, but such scatter is typical in this business. After all, both z_T and z_0 are exponential functions of the measurements they derive from [i.e., see (3)]. Nevertheless, the z_T/z_0 values tend to collect around the theoretical prediction, (8), and decrease with increasing R_*, as the theory predicts.

Andreas (2002), however, points out a problem with plots such as Fig. 5: Because z_0 appears on both axes, the plot is prone to fictitious correlation. To minimize this effect and to reduce the scatter, we replot the z_T values from Fig. 5 in Fig. 6 as averages over u_* bins. In Fig. 6, we also include results from the three PAM stations. In total, Fig. 6 represents over 1,200 hourly eddy-correlation measurements of z_T over snow-covered sea ice.

Although the bin-averaged values in Fig. 6 are still somewhat scattered, they are generally within an order of magnitude of what we would predict z_T to be based on (5) and (8). An order of magnitude uncertainty leads to an uncertainty in C_{HN10} of 15–20%. Figure 6, in combination with other recent test of Andreas's (1987) z_T model, (8) (e.g., Andreas 2002; Denby and Snellen 2002; Andreas et al. 2003), confirms that the model is a useful tool over surfaces of ice and snow.

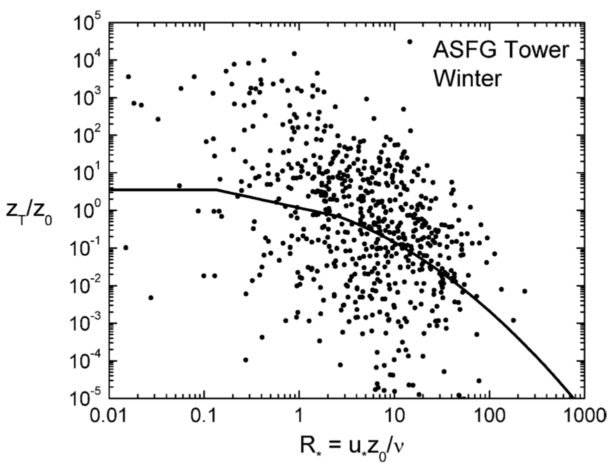

Figure 5. Hourly averages of z_T/z_0 measured on the Atmospheric Surface Flux Group's main SHEBA tower during the winter (i.e., 1 November 1997 through 14 May 1998 and 15–29 September 1998). The curve is (8).

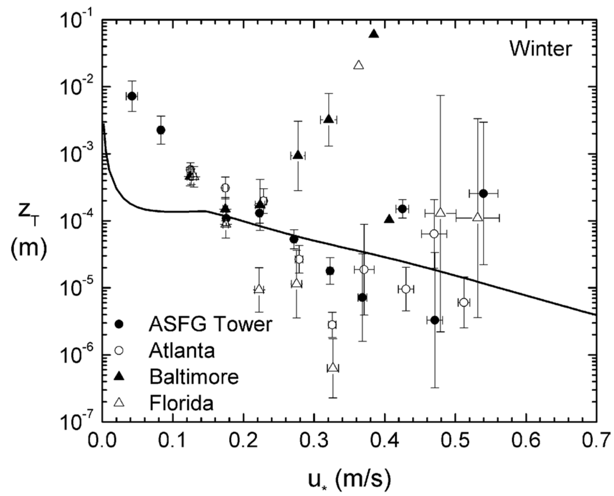

Figure 6. Hourly z_T values from the Atmospheric Surface Flux Group's main tower and from the Flux-PAM stations called Atlanta, Baltimore, and Florida are here averaged in u_* bins that are normally 5 cm s^{-1} wide. The error bars are ± 2 standard deviations in the means of the z_T and u_* values in the bin. Markers without error bars are single values. The curve results from combining (5) and (8).

4.3 z_T in Summer

We present Fig. 7 as a counterpoint to Fig. 5. This shows the z_T/z_0 ratio measured on our main tower during the summer, 15 May–14 September 1998. In contrast to Fig. 6, most of the points in Fig. 7 are above the model prediction. This result implies that the sensible heat fluxes that we measured during the summer were larger in magnitude than what we predict with (1b), (2b), and (8).

We can think of two simple explanations for this mismatch. Either (1b) and (2b) are accurate but (8) underpredicts z_T in summer. Or (8) is still reliable, but something is wrong with (1b) and (2b) during the summer. Because (8) has proved reliable over ice surfaces that were near 0°C (i.e., Denby and Snellen 2002; Andreas 2002, Fig. 3), we lean toward the second explanation.

During the summer, the bare ice surface was near 0°C because of the melting. Surprisingly, though, the water in the melt ponds and leads was significantly warmer than 0°C. For example, Paulson and Pegau (2001) report surface water temperatures in leads in the vicinity of the SHEBA camp of 2°C. In other words, during much of the summer, the surface over which we were sampling

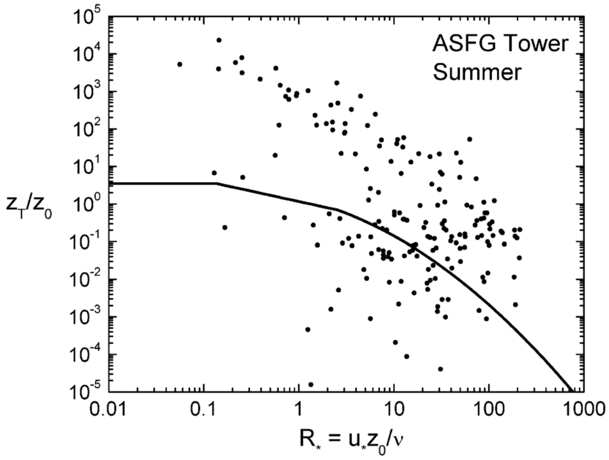

Figure 7. As in Fig. 5, but the z_T/z_0 ratios here were measured during the SHEBA summer, 15 May–14 September 1998.

did not have a uniform temperature. Consequently, (1b) is not strictly accurate.

We can, however, salvage elements of our bulk flux algorithm using a mosaic technique (e.g., Vihma 1995). We simply estimate the areally averaged heat flux as the area-weighted sum over all surfaces:

$$\begin{aligned} H_s &= \rho c_p A_i C_{Hr,i} U_{r,i} \left(\Theta_{s,i} - \Theta_{r,i}\right) \\ &+ \rho c_p A_p C_{Hr,p} U_{r,p} \left(\Theta_{s,p} - \Theta_{r,p}\right) \\ &+ \rho c_p A_L C_{Hr,L} U_{r,L} \left(\Theta_{s,L} - \Theta_{r,L}\right) . \end{aligned} \tag{9}$$

Here, the subscripts i, p, and L refer to conditions over ice, melt ponds, and leads, respectively. Likewise, A_i, A_p, and A_L are the fractional areas of ice, ponds, and leads such that $A_i + A_p + A_L = 1$.

We can implement various methods and assumptions for treating (9). But we are not going to discuss these solutions here. Rather, we simply want to explain how (9) is compatible with Fig. 7.

To start, we can assume that the open water areas are small; they therefore do not induce any local circulations. Consequently, $U_{r,i}$, $U_{r,p}$, and $U_{r,L}$ are all approximately the same, as are $\Theta_{r,i}$, $\Theta_{r,p}$, and $\Theta_{r,L}$. Because during the summer everything is near 0°C, the stratification corrections in $C_{Hr,i}$, $C_{Hr,p}$, and $C_{Hr,L}$ are all comparable. Further, if we assume that the roughness lengths z_0 and z_T depend only weakly on the surface type, we can reduce (9) to

$$H_s = \rho c_p C_{Hr} U_r \left[\left(A_i \Theta_{s,i} + A_p \Theta_{s,p} + A_L \Theta_{s,L}\right) - \Theta_r\right], \tag{10}$$

where U_r and Θ_r are, again, the wind speed and potential temperature at reference height r.

We recognize $A_i \Theta_{s,i} + A_p \Theta_{s,p} + A_L \Theta_{s,L}$ as the areally averaged surface temperature, $\Theta_{s,ave}$. Because $\Theta_{s,p}$ and $\Theta_{s,L}$ are often higher than $\Theta_{s,i}$, which is constrained to be 0°C or less, $\Theta_{s,ave}$ is often higher than $\Theta_{s,i}$. But we used $\Theta_{s,i}$ to compute z_T in Fig. 7. According to (10), this procedure must overestimate z_T whenever $\Theta_{s,ave}$ is above $\Theta_{s,i}$.

In summary, we conclude that Fig. 7 does not mean that (8) is inaccurate during the summer but, instead, that we need to use a mosaic approach to estimate the turbulent heat fluxes when the surface is heterogeneous in temperature. We are still looking for SHEBA data from which we can estimate $\Theta_{s,ave}$ and, thus, test (10) with our summer data.

5. CONCLUSIONS

The eddy-correlation measurements that we made on our main tower and at three remote Flux-PAM sites during SHEBA provided ample data for developing a preliminary version of the SHEBA bulk flux algorithm. From our yearlong series of drag coefficients, we identified two aerodynamic seasons: winter, when snow was available to blow and drift; and summer, when it was not.

For winter, we parameterize z_0 with (5), which shows that z_0 behaves differently in each of three dynamic regimes.

In summer, we recognize that form drag associated with the vertical ice edges surrounding all the open water dominates the air–surface momentum transfer. When we supplement our summer SHEBA data with two other sets that also relate the drag coefficient to ice concentration, we come up with a unified picture of how C_{DN10} depends on ice concentration for the entire range of fractional concentrations, 0 to 1.

For winter, our SHEBA measurements of the roughness length for temperature, z_T, corroborate Andreas's (1987) model, (8). In summer, the surface was more thermally complex; Andreas's model tends to underestimate z_T because we had not accounted for the warm ponds and leads. Our turbulence measurements responded to these, but our calculations of z_T did not include their influence. We conclude that mosaic calculations will probably be necessary to predict the turbulent heat fluxes correctly in summer.

The values of z_0 and z_T that we report have immediate implications for modeling. We find that

z_0 and, thus, C_{Dr} are not constant in either winter or summer (see Figs. 1–4). z_T is likewise not constant (see Figs. 5–7). Constancy of the transfer coefficients is a common assumption in large-scale sea ice models (e.g., Holland et al. 1993; Bryan et al. 1996). Figures 5 and 7 also demonstrate that z_0 and z_T are not generally equal. From (7), this inequality implies that the transfer coefficients for momentum and sensible heat are generally not equal either. Bryan et al. (1996), for example, assume $z_0 = z_T = 40$ mm. Figures 2 and 6 clearly show that both z_0 and z_T over sea ice are one to two orders of magnitude smaller than this value. Finally, comparing Figs. 2 and 6, we see that, generally, $z_0 > z_T$. Equation (7) thus implies that $C_{DN10} > C_{HN10}$. Holland et al. (1993), for example, assume the opposite.

6. ACKNOWLEDGMENTS

The U.S. National Science Foundation supported this work with awards to CRREL, NOAA/ETL, and NPS. The National Science Foundation also supported the work at NCAR. The U.S. Department of the Army provided additional support to Andreas and Jordan through projects at CRREL.

7. REFERENCES

Andreas, E. L, 1987: A theory for the scalar roughness and the scalar transfer coefficients over snow and sea ice. *Bound.-Layer Meteor.*, **38**, 159–184.

____, 1995: Air-ice drag coefficients in the western Weddell Sea: 2. A model based on form drag and drifting snow. *J. Geophys. Res.*, **100**, 4833–4843.

____, 2002: Parameterizing scalar transfer over snow and ice: A review. *J. Hydrometeor.*, **3**, 417–432.

____, W. B. Tucker, III, and S. F. Ackley, 1984: Atmospheric boundary-layer modification, drag coefficient, and surface heat flux in the Antarctic marginal ice zone. *J. Geophys. Res.*, **89**, 649–661.

____, C. W. Fairall, P. S. Guest, and P. O. G. Persson, 1999: An overview of the SHEBA atmospheric surface flux program. Preprints, *Fifth Conf. on Polar Meteorology and Oceanography*, Dallas, TX, Amer. Meteor. Soc., 411–416.

____, K. J. Claffey, C. W. Fairall, P. S. Guest, R. E. Jordan, and P. O. G. Persson, 2002: Evidence from the atmospheric surface layer that the von Kármán constant isn't. Preprints, *15th Symposium on Boundary Layers and Turbulence*, Wageningen, The Netherlands, Amer. Meteor. Soc., 418–421.

____, R. E. Jordan, and A. P. Makshtas, 2003: Parameterizing turbulent exchange over sea ice: The Ice Station Weddell results. *J. Climate*, submitted.

Banke, E. G., S. D. Smith, and R. J. Anderson, 1980: Drag coefficients at AIDJEX from sonic anemometer measurements. *Sea Ice Processes and Models*. R. S. Pritchard, Ed., University of Washington Press, 430–442.

Birnbaum, G., and C. Lüpkes, 2002: A new parameterization of surface drag in the marginal sea ice zone. *Tellus*, **54A**, 107–123.

Brutsaert, W., 1975: A theory for local evaporation (or heat transfer) from rough and smooth surfaces at ground level. *Water Resour. Res.*, **11**, 543–550.

Bryan, F. O., B. G. Kauffman, W. G. Large, and P. R. Gent, 1996: The NCAR CSM flux coupler. NCAR Tech. Note NCAR/TN-424+STR, 48 pp.

Denby, B., and H. Snellen, 2002: A comparison of surface renewal theory with the observed roughness length for temperature on a melting glacier surface. *Bound.-Layer Meteor.*, **103**, 459–468.

Fairall, C. W., E. F. Bradley, D. P. Rogers, J. B. Edson, and G. S. Young, 1996: Bulk parameterization of air-sea fluxes for Tropical Ocean-Global Atmosphere Coupled-Ocean Atmosphere Response Experiment. *J. Geophys. Res.*, **101**, 3747–3764.

Holland, D. M., L. A. Mysak, D. K. Manak, and J. M. Oberhuber, 1993: Sensitivity study of a dynamic thermodynamic sea ice model. *J. Geophys. Res.*, **98**, 2561–2586.

Holtslag, A. A. M., and H. A. R. De Bruin, 1988: Applied modeling of the nighttime surface energy balance over land. *J. Appl. Meteor.*, **27**, 689–704.

Jordan, R. E., E. L Andreas, and A. P. Makshtas, 2001: Modeling the surface energy budget and the temperature structure of snow and brine-snow at Ice Station Weddell. Preprints, *Sixth Conf. on Polar Meteorology and Oceanography*, San Diego, CA, Amer. Meteor. Soc., 129–132.

Liu, W. T., K. B. Katsaros, and J. A. Businger, 1979: Bulk parameterization of air-sea exchanges of heat and water vapor including the molecular constraints at the interface. *J. Atmos. Sci.*, **36**, 1722–1735.

Owen, P. R., 1964: Saltation of uniform grains in air. *J. Fluid Mech.*, **20**, 225–242.

Paulson, C. A., 1970: The mathematical representation of wind speed and temperature profiles in the unstable atmospheric surface layer. *J. Appl. Meteor.*, **9**, 857–861.

____, and W. S. Pegau, 2001: The summertime thermohaline evolution of an Arctic lead: Heat budget of the surface layer. Preprints, *Sixth Conf. on Polar Meteorology and Oceanography*, San Diego, CA, Amer. Meteor. Soc., 271–274.

Persson, P. O. G., C. W. Fairall, E. L Andreas, P. S. Guest, and D. K. Perovich, 2002: Measurements near the Atmospheric Surface Flux Group tower at SHEBA: Near-surface conditions and surface energy budget. *J. Geophys. Res.*, **107** (C10), DOI: 10.1029/2000JC000705.

Schlichting, H., 1968: *Boundary-Layer Theory*. 6th ed. McGraw-Hill, 748 pp.

Smith, S. D., 1988: Coefficients for sea surface wind stress, heat flux, and wind profiles as a function of wind speed and temperature. *J. Geophys. Res.*, **93**, 15,467–15,472.

Vihma, T., 1995: Subgrid parameterization of surface heat and momentum fluxes over polar oceans. *J. Geophys. Res.*, **100**, 22,625–22,646.